Simulation of Friction Stir Extrusion using Smoothed Particle Hydrodynamics (SPH)

Mostafa Akbari*
Department of Mechanical Engineering,
Technical and Vocational University (TVU), Tehran, Iran
E-mail: mo-akbari@tvu.ac.ir
*Corresponding author

Mansour Hakimollahi
Ph.D. Gratuated , Department of Automotive Engineering
Iran University of Science and Technology,

Parviz Asadi
Department of Mechanical Engineering, Faculty of Engineering,
Imam Khomeini International University, Qazvin, Iran

Hossein Rahimi Asiabaraki
Department of Mechanical Engineering,
Technical and Vocational University (TVU), Tehran, Iran

Received: 27 August 2021, Revised: 26 November 2021, Accepted: 05 January 2022

Abstract: This research aims to construct a three-dimensional numerical model for modeling friction stir extrusion using the completely Lagrangian method, smoothed particle hydrodynamics (SPH). For extrusion simulations, the Finite Element Method (FEM) is extensively utilized; however, it has limitations due to excessive element deformation. Because the particle-based method eliminates the usage of volumetric elements, SPH can be a viable alternative. The performance of the SPH model was evaluated using different particle sizes. The results showed that the smaller particle size improves the temperature results as well as the shape of the wire produced. Then the mechanical and microstructural properties of the produced wires were investigated. The results show that the grain size in the center of the wire is larger than its perimeter due to the lower strain rate in this area. Increased strain reduces grain size in the produced microstructure by increasing nucleation sites during recrystallization, as is well known. The wire microhardness in the centre is 121 HV, whereas it is 129 HV in the periphery. Grain size is the main reason of increased hardness near the sample's periphery.

Keywords: CEL, FSBE, Simulation, Microstructural, SPH

How to cite this paper: Mostafa Akbari, Mansour Hakimollahi, Parviz Asadi, and Hossein Rahimi Asiabaraki, “Simulation of Friction Stir Extrusion using Smoothed Particle Hydrodynamics (SPH)”, Int J of Advanced Design and Manufacturing Technology, Vol. 15/No. 2, 2022, pp. 15–22.
DOI: 10.30495/admt.2022.1938910.1310.

Biographical notes: Mostafa Akbari is currently an Assistant Professor at the Department of Mechanical Engineering, Technical and Vocational University (TVU). His current research interest includes FSW, FSP, and FSE. He received his PhD in Mechanical Engineering from Iran University of Science & Technology in 2017. **Mansour Hakimollahi** is PhD graduated of automotive Engineering Department of Iran University of Science and Technology in 2017 and is managing the science and Technology faculty of Ahlul Bayt International University. **Parviz Asadi** is Assistant Professor of Mechanical Engineering at Imam Khomeini International University. He received his PhD in Mechanical engineering from Tehran University in 2015. **Hossein Rahimi Asiabaraki** received his MSc in Mechanical Engineering from KNTU in 2013. He is currently a Lecturer at the Department of Mechanical Engineering, Technical and Vocational University (TVU). His current research interest includes Automotive and ICE.

1 INTRODUCTION

Metal recycling has caught the attention of many governments due to limited resources, environmental protection, and energy savings. Due to the machining process and the generation of metal chips, alloys such as copper, brass, and aluminum, which are widely utilized in numerous industries, are one of the most significant sources of metal loss. These chips are usually melted and reused. As a result, some companies are required to collect the chips and transport them to the casting shops, where they will be rolled, extruded, and other operations to generate the final/usable metal product. With the introduction of novel recycling processes such as Friction Stir Back Extrusion (FSBE), these alloys can now be recycled straight into the product [1-2]. The most common numerical tool for machining analyses is the Finite Element Method (FEM). In the finite element modeling of the FSBE process, substantial strains are present, resulting in severe mesh deformation at various stages [3]. Due to this challenge, two approaches, the Arbitrary Eulerian-Lagrangian (ALE) and the CEL were developed to address stress concentration and avoid mesh distortion during computation. The ALE approach is a sort of finite element networking in which network components in the space are not fixed or attached to the object or material but rather move as needed. This aspect of the ALE approach helps simulate processes in which the material undergoes substantial and severe local deformation and massive unconstrained flow across free borders [4]. Another finite element networking method used in processes with extensive plastic deformation, such as friction stir extrusion, is the CEL method [5]. The sample is modeled with Eulerian relations in this method, which prevents substantial network distortion. Akbari et al. [5] used the coupled Eulerian-Lagrangian (CEL) technique to model the FSBE process. Using a numerical model, they modeled the temperature and flow of the material well during the process. The disadvantage of these advanced FEM methods is their very high computational time. Smoothed Particle Hydrodynamics (SPH) emerged in manufacturing to address such concerns with FEM [6-7].

SPH is a mesh-free approach that was first developed for astrophysics and has now been expanded to the continuum mechanics scale. SPH, unlike FEM, does not require a gridded domain [8-9]. As a result, it can handle free surfaces, changeable boundaries, and moving interfaces. For machining processes, SPH appears to be a viable alternative to FEM. Since SPH eliminates the challenges associated with element distortion, it has been examined in a few studies for extrusion simulations. Lampropoulos et al. [10] used the SPH method to simulate extrusion processes for two different geometries of the die cross-section. According to their results, the calibrated models were able to capture the experimental data with a 10% accuracy for a variety of initial billet temperature and ram speed values. Bagheri et al. [11] improved 3D numerical models of Friction Stir Welding (FSW), and Friction Stir Vibration Welding (FSVW) processes at various welding speeds using SPH. As can be seen, this method has been used to model a number of manufacturing processes, although the capability of this method to model the FSBE process, which has severe plastic deformation, has not been investigated.

In this study, for the first time, the capability of the SPH method in modeling the FSBE process was investigated. Also, using this method, the reasons for microstructural changes in the radial direction of the produced wires, which are shown in experimental works, will be investigated. To begin, The FSBE process was modeled using the SPH method. Then the microstructural and mechanical properties of the produced wires were obtained using experimental methods. The model is employed to study the strain and temperature distribution during the process. By acquiring these data from numerical results, the microstructural and mechanical properties of the produced wires were investigated.

2 MODEL DESCRIPTION

Large strains are present in the finite element modeling of the FSBE process, resulting in severe mesh distortion at various phases. Mesh-based numerical methods, such as early Lagrangian models, fail to account for mesh deformation during simulation [7]. As a result, the advanced mesh-free SPH model was employed to solve the problem in this work. The elements and fixed grid are not constrained to each other in the SPH technique, allowing the workpiece to maintain a high deformation rate during the simulation. As a result, the FSBE is precisely modeled using ABAQUS in EXPLICIT mode. Because the SPH method uses Lagrangian physics, all output fields may be easily traced throughout time. The problem is modeled using the SPH technique by distributing numerical nodes over the stated problem environment and turning the continuous model into a discretized model. In reaction to its effective stress or imposed hydrostatic pressure, each node, on the other hand, moved and accelerated. The effect of each node on its neighbors was calculated using the kernel function. As a result, the SPH method is particularly useful in determining the force, stress, and strain distribution.

FEM codes face a big issue in simulating forming processes in which the material is highly distorted (Plastic deformation process) during the extrusion process. The main problem with utilizing a traditional

FE model with a Lagrangian mesh at high deformation is mesh distortion. Traditional Langrangian techniques have difficulty resolving large deformations [4]. Meshless or meshfree approaches have lately evolved due to these and other shortcomings in standard Langrangian procedures. These methods focus on imposing particular replicating requirements to generate interpolation functions at arbitrary discrete places in the domain, obviating the necessity for elements and a mesh. SPH is a cutting-edge computer simulation technique for continuous media mechanics.

The SPH approach is a total lagrangian first developed for analyzing and simulating astrophysics problems [12]. Later, the method was extended to describe unsteady flows with massive deformations and analyze and simulate situations involving significant strain solid mechanics. The absence of a grid and the discretization of the continuum are the primary distinctions between FEM and SPH. It does not suffer from the mesh distortion problems that limit Lagrangian methods based on the structured mesh when simulating large deformations. Mesh-free numerical integration of partial differential equations is a relatively new numerical approach. There is no direct connection between particles. The particles are the foundation of an interpolator scheme based on the kernel function, which is the method's core and ultimately depends on another key feature: the length of the smoothing [13].

Using kernel interpolation algorithms, the problem variables, such as velocity, density, stresses, and deformation, are examined in the SPH technique based on the weighted average value of numerical nodes over neighboring nodes [14]. As a result, these models can simulate inhomogeneous node distribution tests and massive deformation processes. This method's Lagrangian structure makes it easy to track all field variables across time.

There are various types of interpolation kernel smoothing functions for modeling massive deformation problems, which are chosen based on the physics of the problem. The effective radius of the central element for a finite number of neighbors is generally determined to be roughly 27 and 56 elements in two-dimensional and three-dimensional models, respectively [13]. Furthermore, the scaling factor (λ) can be utilized for the effective radius to raise or reduce the element numbers of neighbors, which directly impacts calculation time and model accuracy.

The current study uses the cubic spline function as an interpolation kernel function to establish discrete points as physical particles. As shown in "Fig. 1", the weighting function of W has a bell-shaped with kernel length of λh. The amount of λ is determined by assuming the summation over all particles with a distance of h from r using a weighted kernel function type. Applying the continuous first derivative in this study, the particles with a range of h from r are considered for the scheme of SPH interpolation summation.

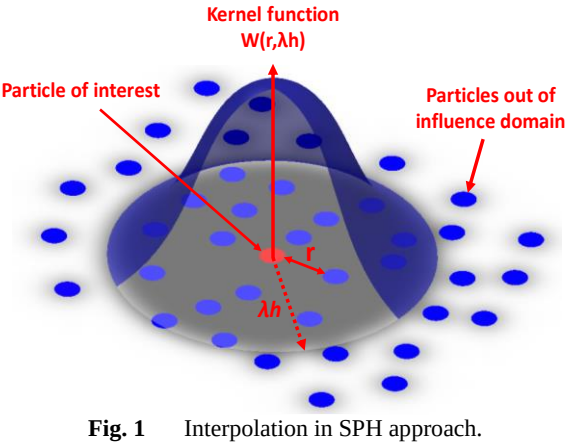

Fig. 1 Interpolation in SPH approach.

By translating the FEM nodes of each element (C3D8R) to SPH particles (PC3D), an equivalent SPH model may be created with this FEM model. It is worth noting that SPH has no physical elements; the FEM nodes are simply turned into SPH particles. As indicated in "Fig. 2", the particle spacing (L) is the same as the FEM element size (b). The volume of each particle is calculated using this spacing, which is twice the "characteristic length" provided in ABAQUS. Typically, evenly distributed particles are recommended in SPH modeling, so a constant L can be employed throughout the model. As a result, to ensure compatibility during the FEM-SPH conversion, all FEM elements were made cubic.

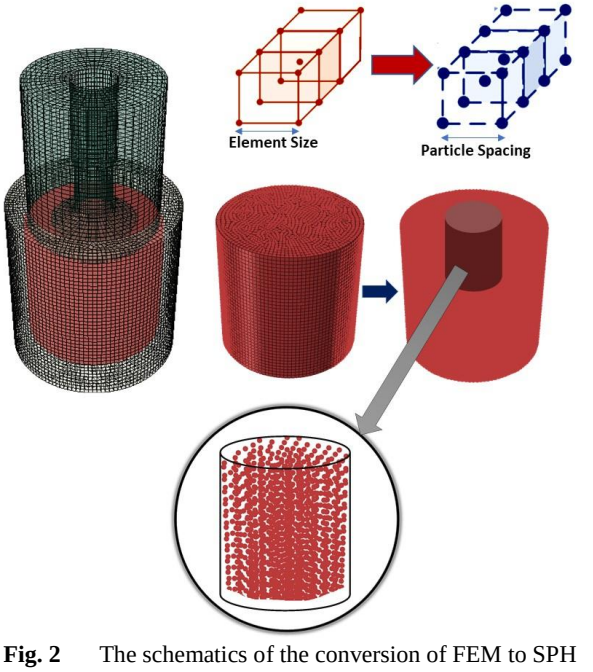

Fig. 2 The schematics of the conversion of FEM to SPH models**.**

As evident in "Fig. 1", the spatial integration is directly carried out at particles. Thus, by considering the weighted sum for the ith node over the jth neighboring nodes and its practical domain, the value of the field variable can be calculated for ith node. The discretized field variable (f) of the ith material node at the spatial location of r_i^a is approximately as follows [13]:

$$r = | r_i^\alpha - r_j^\alpha | \tag{1}$$

Where, ρj and Mj represent density and elements mass, respectively and $W(r, h)$ is an interpolation Kernel function. The vector divergence and scalar gradient are also as follows:

$$\nabla f_i = \sum \frac{M_j}{\rho_j} f_j . \nabla_i W(r_i - r_j, h) \tag{2}$$

And:

$$\nabla f_i^a = \sum_{j=q}^{N_i} \frac{M_j}{\rho_j} f_j^a . \nabla_i W(r_i - r_j, h) \tag{3}$$

The above equations mean summation overall j particles of the particle of interest (i). In addition, choosing the h value (smooth length) and defining the number of j particles (resolution) directly affects the properties of the i particle. As a result, the model is more efficient when the density of local particles determines h. In addition, the mass of particle i in the SPH model is constant and proportional to the $\rho ihi3$. Therefore, the hi can be calculated by [15]:

$$\frac{\partial h_i}{\partial t} = -(\frac{h_i}{3\rho_i}) \frac{\partial \rho_i}{\partial t} \tag{4}$$

To solve the SPH model, a system of ordinary differential equations can be used to rewrite a set of continuum equations [16]. As a result, the material momentum, mass conservation, and energy conservation equations are as follows:

$$\frac{\partial \rho_i}{\partial t} = \rho_i \sum_{j=1}^{N_i} \frac{M_j}{\rho_j} V_{ij} . \nabla_i W(r_i - r_j, h) \tag{5}$$

$$\frac{\partial V_i}{\partial t} = -\sum_{j=1}^{N_i} M (\frac{p_i + p_j}{\rho_i \rho_j} + \prod_{ij}) . \nabla_i W(r_i - r_j, h) + F_i \tag{6}$$

$$\frac{\partial T_i}{\partial t} = -\frac{1}{\rho_i C_{p,i}} \left[\begin{array}{l} \sum_{j=1}^{N_i} \frac{M_j}{\rho_i} \frac{4K_i K_j}{K_i + K_j} \frac{(T_i - T_j)}{|r_{ij}|^2} r_{ij} \nabla_i W(r_i - r_j, h) \\ -\frac{1}{2} \sum_{j=1}^{N_i} M_j \prod_{ij} V_{ij} \nabla_i W(r_i - r_j, h) - RT_i \delta_i \end{array} \right] \tag{7}$$

Where, the Πij, Vij, Fi, pi, R, and K are viscous term, the velocity of particle $ithe$ boundary, force, the fluid pressure at the position ri, heat transfer coefficient, and heat conductivity, respectively. For particles at the boundary and outside the border, the δ is set to one and zero, respectively.

The convective heat transfer coefficient modeled the natural convection heat loss at the matrix and paunch exterior surfaces. The materials in the process have a self-contact in addition to the FSBE paunch/workpiece contact. To account for all contact sites between the workpiece and the tool, a general contact interaction will be used. The Coulomb friction model is used to represent the friction between the tool and the substance. The hard contact pressure enclosure also simulates typical tool-to-material contact, which reduces the penetration of workpiece nodes into the tool.

Temperature, strain rate, and strain are all factors that influence the material flow stress in the process. Therefore, Johnson-Cook's model (JC) is utilized to model the flow of material:

$$\sigma = (A + B\varepsilon^n)(1 + C \ln\left(\frac{\dot{\varepsilon}}{\dot{\varepsilon}}\right))[1 - \left(\frac{(T - T_r)}{(T_m - T_r)}\right)^m \tag{8}$$

Where A, B, C, n, and m are constants related to the material, T_m is melting temperature (from "Table 1"); T_r is the ambient temperature, ε represents the plastic strain; $\dot{\varepsilon}$ is the normalizing strain rate; and $\dot{\varepsilon}$ is the effective plastic strain rate [17-18]. Eq. (7's) first term is the power law, which describes how plastic training affects flow stress. The effects of strain rate and temperature were examined in the second and third terms of the equation. "Table 2" illustrates Johnson-Cook's parameters for brass alloys [17].

Table 1 The constants of JC model for the AA 5083 and brass alloys [17]

Material	Brass
A [MPa]	112
B [MPa]	505
C	0.009
n	0.42
m	1.68
Tref [°C]	25
Tmelt [°C]	916

The sizes of the elements should be considered as essential criteria in the analysis. This is because element size is vital for model convergence and should be investigated by looking at the developed outcomes. A model is employed to explore the mesh size effect, which is discretized into several mesh sizes ranging from fine to rough. Different mesh sizes ranging from 0.8 to 1.2 mm are employed, as shown in "Fig. 3". For all models, elastic-plastic SPH elements (C3D8R) with an eight-node three-dimensional degree of freedom were utilized.

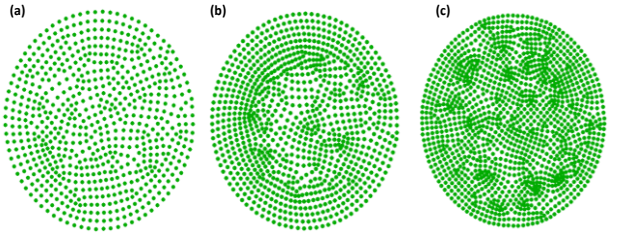

Fig. 3 Different mesh sizes of: (a): 1.2 mm, (b),1 mm, and (c): 0.8 mm.

The rotating tool and matrix are meshed with thermally coupled 4-node 3D bilinear rigid quadrilateral elements as a Lagrangian rigid body. To precisely control tool movement, all tool movement conditions are assigned with regard to the tool reference point ("Fig. 4").

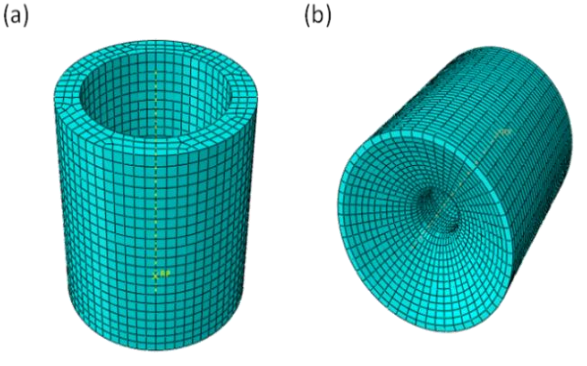

Fig. 4 Lagrangian mesh for: (a): the matrix, and (b): the tool.

3 EXPERIMENTAL PROCEDURE

For a more effortless flow of softened material from the primary material toward the sizing channel for the wire, the tool head has a conical concave toward the central hole. The principal bulk material was a brass shaft with a diameter and height of 30 and 40 mm.

The FSBE procedure was carried out in this study using a CuZn39Pb2Sn brass shaft with the chemical composition stated in "Table 2". H13 steel was used to create the metal matrix, which was subsequently heat treated. After heat treatment, the metal matrix had a hardness of 52 HV ("Fig. 5"). The FSBE tools with an inner diameter of 7mm and an outer diameter of 30mm were made of Chrome-Nickel steel and subjected to heat treatment.

Table 2 Chemical compositions of CuZn39Pb2Sn brass used in this study.

Element	% wt.
Cu	58.9
Zn	37.39
Pb	2.14
Sn	0.60
Fe	0.51
Ni	0.43
Al	0.007
Mn	0.004
Si	0.003
S	0.003
P	0.003

The cross-section of the wires was polished and etched, and their microstructure was investigated using a light microscope to evaluate the microstructure of the created wires. The metallographic samples are etched for 20 seconds in a solution of 5 g Fe_3Cl, 30 mL HCl, and 100 mL ethanol, then washed and dried with distilled water. The hardness of the samples was determined at two spots on the wire: the center and the periphery. A weight of 100 g was applied for 15 seconds during the hardness test. Cometech universal tensile/pressure test equipment was used to perform the standard pressure test at ambient temperature with a strain rate of 10^{-3} s^{-1}. The pressure test specimens were 12 mm long.

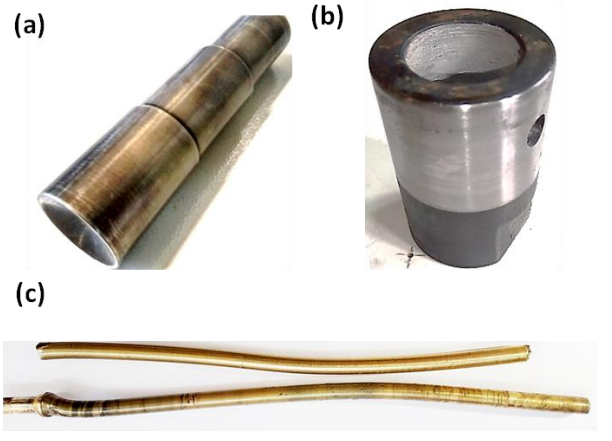

Fig. 5 (a) The tool, (b) The matrix, and (c) some of the produced 7 wires.

4 RESULTS

The temperature distribution in samples is depicted in "Fig. 6". The heat required for the FSBE process is provided by friction between the material and the tool, similar to other friction-based processes. Then, by deformation of the material during the process, the plastic deformation heat is added to the total generated heat. The temperature in the material is around 60 to 90% of the melting temperature because this is a solid-state process [19-20]. As the temperature of the materials rises, they soften, and when an axial force is applied, the softened materials deform and enter the tube. The maximum temperature is reached under the tool shoulder, where the tool has the most force and speed, as shown in "Fig. 6".

As can be seen, the temperature distributions in the models produced with different particle sizes are of good accuracy. In all models, the area where the maximum temperature occurs as well as the maximum temperature value are correctly predicted. As the particle size becomes smaller, the heat transfer inside the material is modeled better, and the area where the maximum temperature occurs is larger. As the particles become finer, the data transfer between the particles improves, which increases the heat transfer from the areas where the heat is generated, such as under the tool shoulder, to other parts of the material. The SPH model has much less computational time (about one-twentieth) than the CEL model [5], which is advantageous for this method.

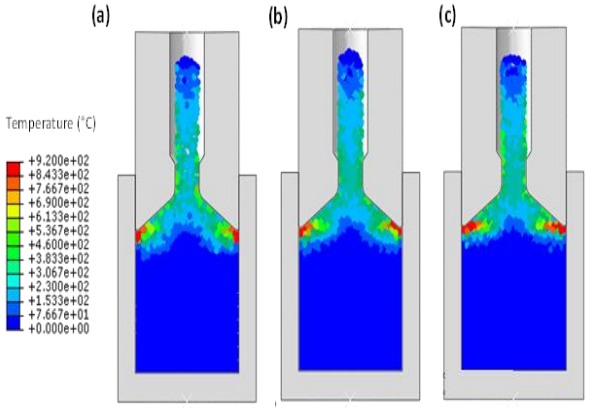

Fig. 6 Temperature distribution in models: (a): SPH with a mesh size of 1.2 mm, (b): SPH with a mesh size of 1 mm, and (c): SPH with a mesh size of 0.8 mm.

Figure 7 shows the shape of the wires produced. It is clear that when using coarse mesh, the wires made show a lot of discontinuity, and the model can not correctly predict the final shape of the wire. As the mesh size becomes smaller, the discontinuities decrease, and the model improves.

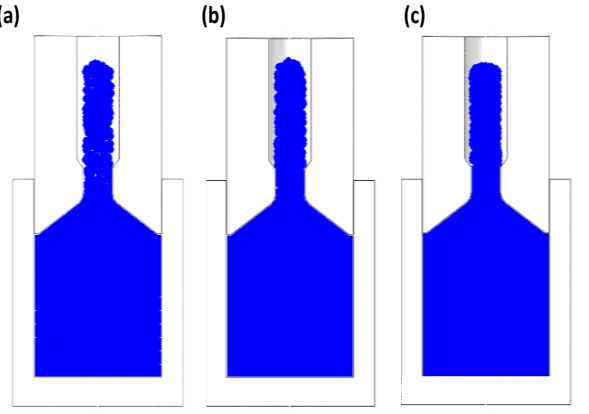

Fig. 7 The shape of the wires produced in the model with the mesh size of: (a):1.2 mm, (b): 1 mm, and (c): 0.8 mm.

Figure 8 shows a cross-section macrograph of the FSBE-produced wire. As shown in this figure, the FSBE method may generate defect-free brass wire by reusing brass chips. Figures 8 illustrate the peripheral and central microstructures of the cross-section of the produced wires by FSBE. The sample has a more refined perimeter microstructure than the center microstructure. This disparity is connected to the amount of strain experienced, which has an impact on microhardness [21].

The materials at the wire periphery are subjected to additional strain due to the tool's increased linear velocity at the wire perimeter rather than at the tool center ("Fig. 9"). Increased strain reduces grain size in the produced microstructure by increasing nucleation sites during recrystallization, as is well known.

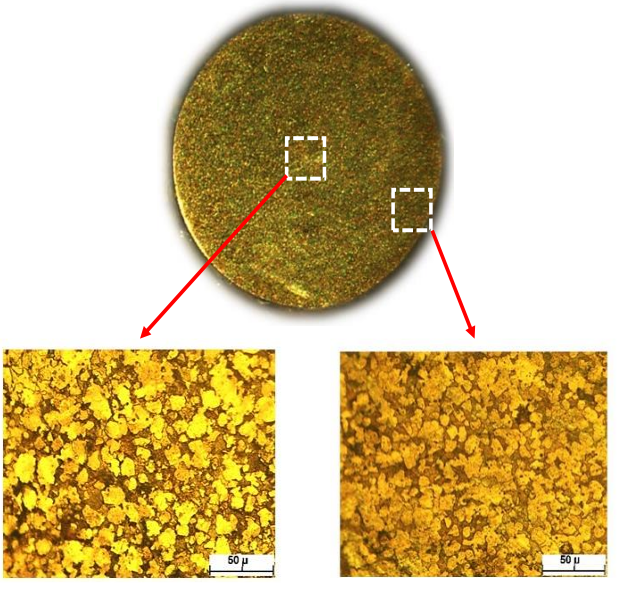

Fig. 8 The microstructure of the center and the perimeter of the wire produced.

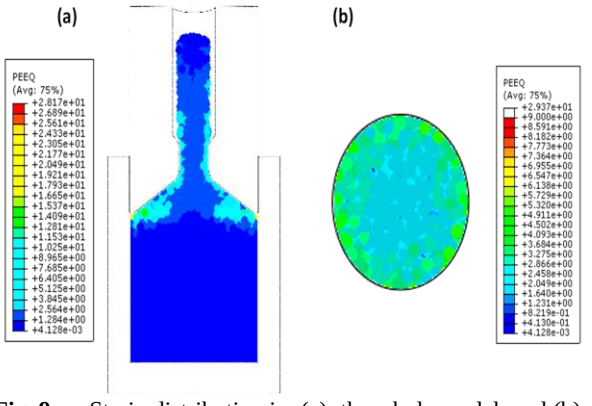

Fig. 9 Strain distribution in: (a): the whole model, and (b): in the cross-section of the wire.

The microhardness value in the sample perimeter should be higher than that in the sample core based on microstructural data. A sample's microhardness in the center is 121 HV, whereas the peripheral microhardness is 129 HV. Greater hardness near the sample's periphery is mainly caused by grain size ("Fig. 8"). The engineering stress-strain pressure test curves are also shown in "Fig. 10".

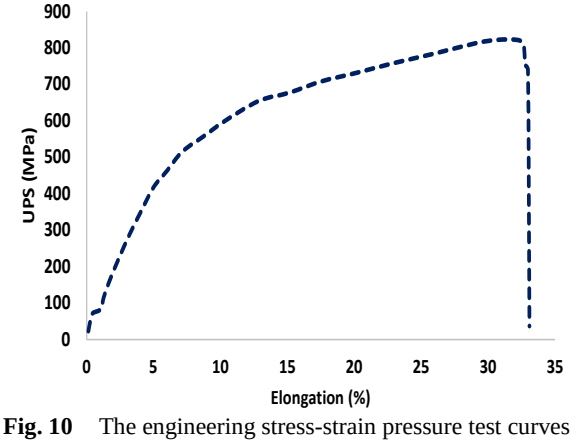

Fig. 10 The engineering stress-strain pressure test curves

7 CONCLUSION

In this study, the FSBE process was investigated using the SPH method, and the performance of this method was investigated. Then the mechanical and microstructural properties of the produced wires were investigated. In summary, the following results were obtained from this study.

- The maximum temperature is reached under the tool's shoulder, where the tool has the most force and speed.
- Lower temperature and higher strain on the surface of the wires reduce the grain size in this area compared to the center of the wire.
- The SPH model predicted the temperature well in the process area, although heat transfer to other areas was not properly modeled.
- Particle size in the SPH model has a considerable impact on the accuracy of the final model.

REFERENCES

[1] Evans, W. T., Gibson, B. T., Reynolds, J. T., Strauss, A. M., and Cook, G. E., Friction Stir Extrusion: A New Process for Joining Dissimilar Materials, Manufacturing Letters, Vol. 5, 2015, pp. 25-8.

[2] Buffa, G., Campanella, D., Fratini, L., and Micari, F., AZ31 Magnesium Alloy Recycling Through Friction Stir Extrusion process, International Journal of Material Forming, Vol. 9, 2016, pp. 613-8.

[3] Akbari, M., Asadi, P., Behnagh, R. A., Modeling of Material Flow in Dissimilar Friction Stir Lap Welding of Aluminum and Brass Using Coupled Eulerian and Lagrangian Method, The International Journal of Advanced Manufacturing Technology, Vol. 113, 2021, pp. 721-34.

[4] Akbari, M., Shojaeefard, M. H., Asadi, P., and Khalkhali, A., Wear Performance of A356 Matrix Composites Reinforced with Different Types of Reinforcing Particles, Journal of Materials Engineering and Performance, Vol. 26, 2017, pp. 4297-310.

[5] Asadi, P., Akbari, M., Numerical Modeling and Experimental Investigation of Brass Wire Forming by Friction Stir Back Extrusion, The International Journal of Advanced Manufacturing Technology, 2021.

[6] Dao, M. H., Lou, J., Simulations of Laser Assisted Additive Manufacturing by Smoothed Particle Hydrodynamics, Computer Methods in Applied Mechanics and Engineering, Vol. 373, 2021, pp. 113491.

[7] Meier, C., Fuchs, S. L., Hart, A. J., and Wall, W. A., A Novel Smoothed Particle Hydrodynamics Formulation for Thermo-Capillary Phase Change Problems with Focus on Metal Additive Manufacturing Melt Pool Modeling, Computer Methods in Applied Mechanics and Engineering, Vol. 381, 2021, pp. 113812.

[8] Zhang, C., Wang, J., Rezavand, M., Wu, D., and Hu, X., An Integrative Smoothed Particle Hydrodynamics Method for Modeling Cardiac Function, Computer Methods in Applied Mechanics and Engineering, Vol. 381, 2021, pp. 113847.

[9] Fuchs, S. L., Meier, C., Wall, W. A., and Cyron, C. J., A Novel Smoothed Particle Hydrodynamics and Finite Element Coupling Scheme for Fluid–Structure Interaction: The Sliding Boundary Particle Approach, Computer Methods in Applied Mechanics and Engineering, Vol. 383, 2021, pp. 113922.

[10] Lampropoulos, A. D., Manolakos, D. E., Application of SPH Method for Modeling of Metal Extrusion Process, Computational Particle Mechanics, 2021.

[11] Bagheri, B., Abdollahzadeh, A., Abbasi, M., and Kokabi, A. H., Numerical Analysis of Vibration Effect on Friction Stir Welding by Smoothed Particle Hydrodynamics (SPH), The International Journal of Advanced Manufacturing Technology, Vol. 110, 2020, pp. 209-28.

[12] Gingold, R. A., Monaghan, J. J., Smoothed Particle Hydrodynamics: Theory and Application to Non-Spherical Stars, Monthly Notices of the Royal Astronomical Society, Vol. 181, 1977, pp. 375-89.

[13] Ansari, M. A., Abdi Behnagh, R., Numerical Study of Friction Stir Welding (FSW) Plunging Phase Using Smoothed Particle Hydrodynamics (SPH), Modelling and Simulation in Materials Science and Engineering, Vol. 27, 2019.

[14] Bonet, J., Lok, T. S. L., Variational and Momentum Preservation Aspects of Smooth Particle Hydrodynamic Formulations, Computer Methods in Applied Mechanics and Engineering, Vol. 180, 1999, pp. 97-115.

[15] Kajtar, J., Monaghan, J. J., SPH Simulations of Swimming Linked Bodies, Journal of Computational Physics, Vol. 227, 2008, pp. 8568-87.

[16] Monaghan, J. J., Smoothed Particle Hydrodynamics, Reports on Progress in Physics, Vol. 68, 2005, pp. 1703-59.

[17] Meyghani, B., Awang, M., Emamian, S., Nor, M., and Pedapati, S. R., A Comparison of Different Finite Element Methods in the Thermal Analysis of Friction Stir Welding (FSW), Metals, Vol. 7, 2017, pp. 450.

[18] Chakrabarty, R., Song, J., A Modified Johnson-Cook Material Model with Strain Gradient Plasticity Consideration for Numerical Simulation of Cold Spray Process, Surface and Coatings Technology, Vol. 397, 2020, pp. 125981.

[19] Balu Mahandiran, M., Vigneshkumar, M., Ashoka Varthanan, P., Abishek, S., Abdulriyazdeen, A., and Abilash, S., Investigation of Solid State Welding of Copper Nickel Alloy (Cu-Ni 90/10) Using FSW Process, IOP Conference Series: Materials Science and Engineering, Vol. 1145, 2021, pp. 012112.

[20] Wang, X., Gao, Y., McDonnell, M., and Feng, Z., On the Solid-State-Bonding Mechanism in Friction Stir Welding., Extreme Mechanics Letters, Vol. 37, 2020, pp. 100727.

[21] Akbari, M., Khalkhali, A., Keshavarz, S. M. E., and Sarikhani, E., Investigation of the Effect of Friction Stir Processing Parameters on Temperature and Forces of Al–Si Aluminum Alloys, Proceedings of the Institution of Mechanical Engineers, Part L: Journal of Materials: Design and Applications, Vol. 232, 2015, pp. 213-29.